Chaplins of Streptomyces coelicolor self-assemble into two distinct functional amyloids

Bokhove, Marcel; Claessen, Dennis; de Jong, Wouter; Dijkhuizen, Lubbert; Boekema, Egbert J.; Oostergetel, Gert T.

Published in:
Journal of Structural Biology

DOI:
10.1016/j.jsb.2013.08.013

Publication date:
2013

Journal of Structural Biology 184 (2013) 301–309

Contents lists available at ScienceDirect

Journal of Structural Biology

journal homepage: www.elsevier.com/locate/yjsbi

Regular Article

Chaplins of *Streptomyces coelicolor* self-assemble into two distinct functional amyloids

Marcel Bokhove [a], Dennis Claessen [b,1], Wouter de Jong [b], Lubbert Dijkhuizen [b], Egbert J. Boekema [a], Gert T. Oostergetel [a,*]

[a] Electron Microscopy, Groningen Biomolecular Sciences and Biotechnology Institute (GBB), University of Groningen, Nijenborgh 7, 9747 AG Groningen, The Netherlands
[b] Microbial Physiology, Groningen Biomolecular Sciences and Biotechnology Institute (GBB), University of Groningen, Nijenborgh 7, 9747 AG Groningen, The Netherlands

ARTICLE INFO

Article history:
Received 29 April 2013
Received in revised form 23 August 2013
Accepted 27 August 2013
Available online 5 September 2013

Keywords:
Streptomyces
Amyloid
Chaplin
Cross-beta structure
Cryo-electron tomography
Electron diffraction

ABSTRACT

Chaplins are small, secreted proteins of streptomycetes that play instrumental roles in the formation of aerial hyphae and attachment of hyphae to surfaces. Here we show that the purified proteins self-assemble at a water/air interface into an asymmetric and amphipathic protein membrane that has an amyloid nature. Cryo-tomography reveals that the hydrophilic surface is relatively smooth, while the hydrophobic side is highly structured and characterized by the presence of small fibrils, which are similar to those observed on the surfaces of aerial hyphae. Interestingly, our work also provides evidence that chaplins in solution assemble into amyloid fibrils with a distinct morphology. These hydrophilic fibrils strongly resemble the structures known to be involved in attachment of *Streptomyces* hyphae to surfaces. These data for the first time show the assembly of bacterial proteins into two distinct amyloid structures that have different and relevant functions *in vivo*.

1. Introduction

Amyloid structures are formed by polypeptides that polymerize into fibrillar assemblies with a cross-β quaternary structure; that is, the fibrils contain extended β-sheets parallel to the fiber axis, with the H-bonded β-strands perpendicular to the axis (Eanes and Glenner, 1968; Kirschner et al., 1987; Jahn et al., 2010). Deposition of amyloid fibers is often associated with neurodegenerative diseases, such as Alzheimer's, Parkinson's, type-2 diabetes, cystic fibrosis and many others (Stefani, 2004; Chiti and Dobson, 2006; Eisenberg et al., 2006). However, many organisms use the cross-β self-organizing principle to create a strong, yet pliable material, which in many instances has a function in adhesion or as protective coating. These functional amyloids are found in mammals, invertebrates, fungi and, not least, bacteria, in which the occurrence of amyloids may be the rule rather than the exception (Fowler et al., 2007; Otzen and Nielsen, 2008; Maury, 2009).

Functional amyloids involved in adhesion are for example curli, extracellular filamentous structures found on the cell surface of *Escherichia coli* and other *Enterobacteriaceae* (Epstein and Chapman, 2008; Shewmaker et al., 2009), and MTP, pili formed by the gram-positive bacterium *Mycobacterium tuberculosis* (Alteri et al., 2007). Protective layers based on amyloids are found in many different organisms. The egg envelope of the annual killifish *Austrofundulus limnaeus* is composed of amyloid fibrils with a diameter of 4–6 nm, strongly reducing water loss under desiccating conditions (Podrabsky et al., 2001). Aerial hyphae of filamentous fungi are coated with an amphipathic layer of hydrophobin rodlets, which has an amyloidal nature and renders the surface strongly hydrophobic. It allows fungi to escape from an aqueous environment and mediates attachment to solid substrates (Wösten et al., 1994a,b).

A similar layer is found on aerial hyphae of the streptomycete *Streptomyces coelicolor*. This Gram-positive filamentous bacterium forms a network of interconnected hyphae within the soil, analogous to the mycelium formed by filamentous fungi. After a period of vegetative growth, aerial hyphae are formed that give rise to small reproductive compartments called spores. Three types of secreted proteins are important in aerial hyphae formation: SapB (Willey et al., 1991, 1993), chaplins (Claessen et al., 2003; Elliot et al., 2003) and rodlins (Claessen et al., 2002, 2004). SapB is secreted as a 21-amino acid amphiphilic peptide (Kodani et al., 2004). Its main function is to enable hyphae to overcome the water surface tension of the aqueous environment facilitating the escape of hyphae into the air. Unlike vegetative hyphae, the outer surface

* Corresponding author.
E-mail addresses: marcel.bokhove@gmail.com (M. Bokhove), d.claessen@biology.leidenuniv.nl (D. Claessen), wouter@elabjournal.com (W. de Jong), l.dijkhuizen@rug.nl (L. Dijkhuizen), e.j.boekema@rug.nl (E.J. Boekema), g.t.oostergetel@rug.nl (G.T. Oostergetel).
[1] Present address: Molecular Biotechnology, Institute Biology Leiden (IBL), Leiden University, Sylviusweg 72, 2300 RA Leiden, The Netherlands.

1047-8477/$ - see front matter © 2013 Elsevier Inc. All rights reserved.
http://dx.doi.org/10.1016/j.jsb.2013.08.013

of aerial structures is hydrophobic and decorated with a proteinaceous layer, known as the rodlet layer. This layer consists of a mosaic of parallel rods, which are up to 450 nm in length and 18–20 nm wide, and are usually paired, with each track supposedly containing two smaller fibrils (Claessen et al., 2004). Atomic force microscopy (AFM) analysis indicated that this layer is initially relatively disorganized, and that the most tightly organized rodlets are evident on the surface of mature spores (Del Sol et al., 2007). Formation of the rodlet layer requires the activity of the rodlin and chaplin proteins. In a Δ*rdlAB* strain, lacking the genes encoding the rodlin proteins RdlA and RdlB, the organization of the rodlet layer was affected (Claessen et al., 2002). Instead of rodlets, a layer of fine fibrils with a diameter of 4–6 nm was observed at the outer surface of aerial hyphae (Claessen et al., 2003). These fibrils are composed of chaplins. *S. coelicolor*secretes eight chaplin proteins (Elliot et al., 2003); five of these chaplins (ChpD–H) are ~55 amino acids long, whereas ChpA–C are ~225 amino acids in length. The fibrils contain one (ChpD–H) or two (ChpA–C) so-called chaplin domains (19). The short chaplins can be further subdivided on the basis of their abilities to form intramolecular disulfide bonds: ChpD, -F, -G, and -H contain two Cys residues, while ChpE has none (Elliot et al., 2003; Di Berardo et al., 2008). Like *in vivo*, mixtures of purified TFA-extractable chaplins (ChpD–H) also assemble *in vitro* at a hydrophobic–hydrophilic interface into a film composed of small fibrils resembling those present at aerial structures of Δ*rdlAB* mutants. These data imply that rodlins are involved in organizing the chaplin fibrils into rodlets. The long chaplins (ChpA–C) are probably necessary to anchor this protein layer to the cell wall, as they contain a sequence that is specifically recognized by sortase enzymes, which covalently couple their substrates to the peptidoglycan layer (Claessen et al., 2003; Elliot et al., 2003; Flärdh and Buttner, 2009; Duong et al., 2012).

Chaplins are also involved in attachment of *Streptomyces* hyphae to surfaces (de Jong et al., 2009). Attachment coincides with the formation of a network of fimbriae, which were shown to be composed of assembled chaplins. Interestingly, hyphal attachment and fimbriae formation were largely prevented when the amyloid-inhibitor Congo red was added to the cultures. This suggests that chaplin amyloids mediate attachment. However, more direct biophysical methods such as X-ray and electron diffraction are required to prove a structure being amyloid.

Detailed diffraction work has been done on different amyloids showing that the β-strands in the β-sheet give a specific meridional diffraction peak at 1/0.47 nm^{-1} (Sunde et al., 1997; Makin and Serpell, 2005; Kwan et al., 2006). Additionally, a 1/0.94 nm^{-1} reflection can be observed in the case of antiparallel β-strands in the cross-β structure (Serpell and Smith, 2000). In some types of amyloid fibers the β-sheets are stacked or paired, giving an additional repeat of 1.0–1.2 nm perpendicular to the 0.47 nm repeat (Makin and Serpell, 2005; Serpell, 2000). Being all based on the cross-β structure, different fiber morphologies have been reported. An example of an amyloid fiber is that formed by the SH3 domain of phosphatidylinositol-3′-kinase (Jiménez et al., 1999). This amyloid fiber is helical and it consists of four protofilaments (thin fibrils). These filaments are built up from hydrogen bonding β-strands forming two β-stacked sheets. Other amyloids are based on β-barrels or β-solenoids in a head-to-tail arrangement (Kwan et al., 2006; Ritter et al., 2005; Wasmer et al., 2008). For the type-I hydrophobin EAS a detailed model has been proposed for the 3 nm protofilaments, based on solution-NMR (Kwan et al., 2006, 2008).

Here we performed a structural study of chaplin assembly using several transmission electron microscopy (EM) techniques, including electron diffraction and cryo-electron tomography. Our work demonstrates that the chaplin proteins assemble at a water/air interface into an amphipathic protein membrane, which has an amyloidal nature and is highly asymmetric. We furthermore show that chaplins assemble in solution into distinct amyloid-like hydrophilic fibers. Chaplins therefore display the unique feature of being able to assemble into two morphologically distinct functional amyloids.

2. Materials and methods

2.1. Extraction of chaplins from Streptomyces coelicolor

Chaplins were extracted with trifluoroacetic acid (TFA) from SDS-treated cell walls of sporulating cultures of the *S. coelicolor* Δ*rdlAB* strain (Claessen et al., 2004), as described (Claessen et al., 2002; Wösten et al., 1993). TFA extracts were taken up in water (1 ml water per mg cell wall powder) and, if necessary, adjusted to pH 7 with diluted ammonia. Chaplin monomers obtained in this way were still functional, as described previously (Claessen et al., 2003; Elliot et al., 2003; Sawyer et al., 2011).

2.2. Electron microscopy and specimen preparation

EM specimens of chaplins were prepared by air-drying freshly prepared chaplin solutions (20–200 μg ml^{-1}) on Butvar-coated grids or by adsorbing chaplin fibers formed in solution to carbon coated grids. Alternatively, chaplins were allowed to assemble at the air–water interface of a droplet on copper EM grids covered with a holey carbon support film. After 15 min, the excess of solvent together with the chaplin films assembled at the bottom side of the holey carbon grid, were removed by blotting from underneath the EM grid. Contrast enhancement was done by negative staining with 2% uranyl acetate or by platinum shadowing in an Edwards 306a evaporation device under an angle of 30°, thereby taking care that identical amounts of metal were deposited on either side of the EM grid. Stained and shadowed samples were investigated using a Jeol JEM-1200EX electron microscope at an acceleration voltage of 100 kV or a CM120 Philips TEM microscope equipped with a Gatan UltraScan SP 4K cooled CCD camera. Images were recorded at 20,000–60,000× magnification on Kodak SO-163 electron image film or CCD camera.

Cryo-TEM was used to investigate unstained monolayers and fibers formed in solution on holey carbon. For monolayers diluted chaplin solutions were assembled on an EM grid with a holey carbon support film and washed (from the back-side of the grid) with 50 mM ammonium acetate containing 2% trehalose. Preformed fibers were briefly adsorbed to the holey carbon film. After blotting the grids to remove the remaining solution, the specimens were plunge-frozen in liquid ethane using a Reichardt-Jung KF-80 or FEI Vitrobot freezing device. Grids were investigated in a CM120 Philips TEM microscope equipped with a Gatan UltraScan SP 4K cooled CCD camera or a Tecnai G2 Polara cryo-electron microscope (FEI) equipped with an Gatan imaging energy filter (GIF). Images were recorded at 120 or 300 kV acceleration voltage, at 34,000–47,000× magnification and a defocus value around 2 μm. Selected area electron diffraction patterns were recorded at 120 kV or 300 kV and a camera length of 1.25–1.6 m. When diffraction and imaging was done on the same area, electron diffraction was done prior to imaging, because diffraction requires a lower electron dose than imaging, resulting in less radiation damage if the area is sufficiently large (⩾1 μm diameter). Asbestos crystals were used as an external standard to deduce the relative orientation between a diffraction pattern and the corresponding image.

For electron tomography, specimens were prepared on holey carbon grids, and either air-dried followed by platinum shadowing from two sides, or frozen-hydrated as for Cryo-EM. 10 nm gold particles were added as fiducial markers. Tilt series from −60° to +60° were recorded in a 300 kV G2 Polara electron microscope (FEI)

equipped with a Gatan post-column energy filter. Images were recorded with a 2k × 2k CCD camera (Gatan) at 4 μm defocus (first CTF zero at 2.8 nm) and 51,700×magnification, resulting in a pixel of 0.58 nm at the level of the specimen. Tilt series were recorded at 2° increments with a total dose of about 8000 electrons/nm^2. Tomograms were calculated using IMOD software (Kremer et al., 1996).

For atomic force microscopy (AFM) a diluted chaplin solution was applied to freshly cleaved (hydrophilic) mica. After 20 min, the solvent underneath the assembled film was carefully blotted away from the edges of the drop such that the film settled on the mica. After drying the samples for 20 min in air, the hydrophobic air-exposed side of the film was analyzed on a Digital Instruments EnviroScope AFM (Veeco Instruments Inc., Santa Barbara, CA, USA), equipped with a NanoscopeIIIa controller in tapping mode. The probe used was a VEECO SNL-10A probe with a nominal spring constant of 0.35 Nm^{-1} and a resonant frequency of 50–80 kHz, as specified by the manufacturer. Height images were processed using the Free Open Source software package Gwyddion (Necas and Klapetek, 2012).

3. Results

Fibrils formed by the *S. coelicolor* chaplin proteins were studied by transmission electron microscopy. We focused our research on two biologically relevant situations. First, we characterized fibrils assembled at the air–water interface, simulating those formed at the hydrophobic–hydrophilic interface between the cell wall of aerial hyphae and the air. Secondly, we studied fibrillar structures formed in solution, which resemble the fimbrial structures observed between hyphae adhering to hydrophobic solid substrates (de Jong et al., 2009).

3.1. Assembly of chaplins into an amphipathic and asymmetric protein membrane

When a diluted chaplin solution is dried down onto a solid hydrophobic support, a mosaic of flexible fibrous structures of different lengths is formed, as visualized by shadowing with platinum (Pt) (Fig. S1). These fibrils resemble those present on the outer surface of spores of Δ*rdlAB* mutants of *S. coelicolor*, as shown previously (Claessen et al., 2003 and Fig. S2). Although these images of air-dried chaplin solutions show the presence of fibrils, their precise origin remains unclear. They could have been formed on the hydrophobic support, in solution, or at the air–water interface. *In vivo* assembly of these proteins occurs predominantly at hydrophilic–hydrophobic interfaces, such as those between the (hydrophilic) cell wall and the (hydrophobic) air, or at the interface between the aqueous environment and the air. Therefore, chaplins were allowed to assemble at the air–water interface of a droplet of a chaplin-containing solution. Samples were mounted on an EM grid covered with a holey carbon support film (see experimental procedures for more details). Following assembly and blotting, the specimen was shadowed from either side (Fig. 1A). Analysis of these samples by TEM showed that the fibrils formed an intact film with a strong asymmetric topology. The hydrophobic side of the film, facing the air, appeared very structured and was composed of thin fibers ranging in length from less than 100 to 1 μm (Fig. 1B and C). In contrast, the hydrophilic side, facing the solvent, appeared unstructured (Fig. 1D and E). From the hydrophobic side the chaplin film extended from the hole (h) over the carbon support film (c), whereas from the hydrophilic side the chaplin film was only visible through the hole (h). This indicates that no rearrangement of the asymmetric film takes place during preparation and that the two surfaces can be studied separately. Indeed, when the assembled chaplin protein film was picked up from the surface of a droplet with a hydrophobic holey support film and shadow-casted from the backside (Fig. 1F), the fibrous hydrophobic surface was only visible through the holes. The width of the fibrils observed at the hydrophobic side was 7–8 nm, similar to those observed after drying down an aqueous chaplin solution onto a Butvar support film (Fig. S1). In addition to the fibrils, larger aggregates were visible in the chaplin film preparations (arrows in Fig. 1B and D). Most aggregates seemed to be attached to the hydrophilic side. They were also visible from the hydrophobic side, because of their effect on the flatness of the assembled chaplin film (Fig. 1C).

We also negatively stained the hydrophilic side to reveal details that might have been lost during air-drying, preceding shadow casting with Pt. Therefore, chaplin films were assembled at the air–water interface on a holey carbon support film as before, and stained with uranyl acetate from the hydrophilic side. In the electron micrographs the fibrillar structure, seen so clearly after shadowing the opposite (hydrophobic) side, was only very weakly visible (Fig. 1G). No periodic details in the direction of the fibers could be seen by Fourier transformation or by averaging segments of fibrils by single-particle analysis methods (data not shown).

To further substantiate the asymmetry observed in the Pt-shadowed chaplin film, electron tomography was used, which also allowed us to reconstruct the 3D volume of the chaplin layer sandwiched between two Pt-layers. Analysis of the different slices of the reconstructed volume showed the typical fibrillar morphology associated with the hydrophobic side (Fig. 2A), with fibril widths of 7–8 nm. Approximately two slices below the fibrillar layer, before entering the Pt layer, a relatively smooth layer was observed (Fig. 2B). This layer represents the hydrophilic side of the chaplin film as observed before. The observation that the distance between the hydrophobic and hydrophilic layer is two slices indicated that the dehydrated, shadowed chaplin layer is approximately 2 nm thick.

The 3-dimensional reconstruction of the Pt-shadowed chaplin fibril film gave an indication of the thickness in the dehydrated state. To reconstruct the 3D-volume of the native, hydrated chaplin film, cryo-electron tomography was used. The tomographic reconstruction of a chaplin film on vitreous ice revealed a similar morphology as Pt-shadowing: the hydrophobic side is structured with a mosaic of 7–8 nm-wide fibrils (Fig. 3A, arrows) while the hydrophilic side is relatively smooth with small protrusions (Fig.3B arrow heads; Supplementary movie S1). Interestingly, the distance between the fibrillar layer on the hydrophobic side and the hydrophilic side was approximately six slices. This suggested that the thickness of the hydrated chaplin fiber film is approximately 7 nm. The thickness of the native hydrated chaplin film deviated significantly from the thickness as observed in the dried Pt-shadowed state. To verify that the hydration state of the chaplin film affects the height, tapping-mode AFM was applied to assembled chaplin films, settled and dried on mica. Also AFM images of chaplin films showed the typical mosaic of 8 nm-wide fibrils (Fig. 4). Height measurements indicate that in a dried state the chaplin fibril height was only 1.5 ± 0.1 nm (Fig. 4), consistent with the measurements of dried Pt-shadowed films.

Taken together, shadowing and negative staining show that the two sides of the chaplin film have a distinct ultrastructure, with the hydrophilic side being rather flat and unstructured and the hydrophobic side showing a mosaic of fibrils. In addition, cryo-electron tomographic reconstructions indicated that the native hydrated chaplin fibril film is 7 nm thick.

3.2. Chaplins assembled at the air–water interface are amyloid

Because negative staining with uranyl acetate did not give any detailed information about the hydrophilic side of chaplin films

and tomography and shadowing with Pt only gave very low resolution information, we decided to use cryo-TEM to get more details about the chaplin film assembled at the air–water interface. Films formed in about 20 min were mounted on holey carbon-coated EM grids as for shadowing, blotted and flash-frozen in liquid ethane. The hydrophilic side of the resulting film was covered with a thin amorphous ice layer, thereby preventing formation of drying artifacts. A representative electron micrograph is presented in Fig. 5A. The inset in Fig. 5A shows a calculated diffraction pattern of the boxed area. A 7.3 ± 0.2 nm repeat was visible perpendicular to the fibril axes, corresponding to the diameter of one fiber. No smaller details in the direction of the fibril axis were observed in the images. To get higher-resolution information on how a fibril is constructed, we used electron diffraction. The diffraction pattern in Fig. 5B shows a sharp ring at 1/0.47 nm^{-1}, resulting from diffraction peaks from differently oriented fibrils. The distance of 0.47 nm strongly indicates that hydrogen-bonded β-strands forming β-sheets are present in the plane of the film (Fig.5B), consistent with other amyloid proteins (Sunde et al., 1997; Makin and Serpell, 2005). To deduce the orientation of the 0.47 nm periodicity relative to the direction of the fibril we recorded both selected-area electron diffraction patterns and images of the same areas. Fig. 6A shows an area with partially aligned fibers, leading to a partially oriented diffraction pattern calculated from the image (Fig. 6B). The arrow indicates the direction perpendicular to the predominant fibril orientation in Fig. 6A. The electron diffraction pattern of the same area, recorded before the image, showed a similar predominant orientation of the 0.47 nm spacing (arrow, Fig. 6C), which is perpendicular to the 7.3 nm spacing and thus in the direction of the fibril axis. This is direct evidence for the presence of a cross-β structure in the chaplin fibril films, proving that chaplins assemble into amyloid fibrils at the air–water interface. In the

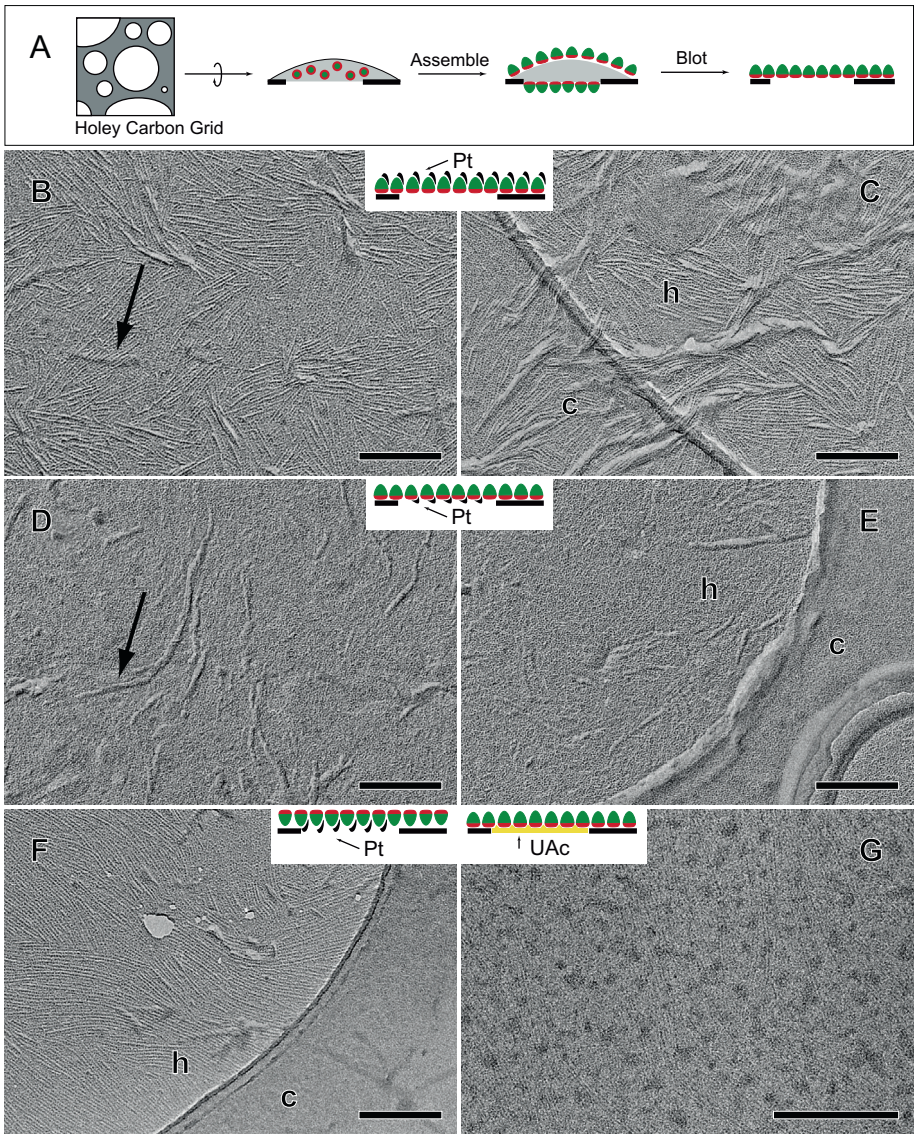

Fig.1. Electron microscopy of chaplin fibril films formed at the air–water interface of a chaplin protein solution. (A) A droplet of monomeric chaplins in water is placed on a holey carbon coated EM grid, left to assemble, and blotted from below through the holes in the carbon film to remove the solvent and the film assembled at the backside in the holes. (B) Chaplin film spanning a hole in the support film, shadowed from the hydrophobic (air-exposed) side. (C) Detail of the film as in B, at the edge of a hole. The fibers continue from the hole (h) onto the carbon film (c). (D) Chaplin film spanning a hole in the support film, shadowed from the hydrophilic solvent-exposed side. (E) As in D. The chaplin film is only visible through the hole (h) in the carbon film (c). (F) Chaplin film picked up from the surface of a droplet with a hydrophobic holey carbon coated grid and shadowed with Pt from the backside of the grid. (G) Chaplin film negatively stained from the hydrophilic side with uranyl acetate. The scale bar for frames B–G represents 200 nm.

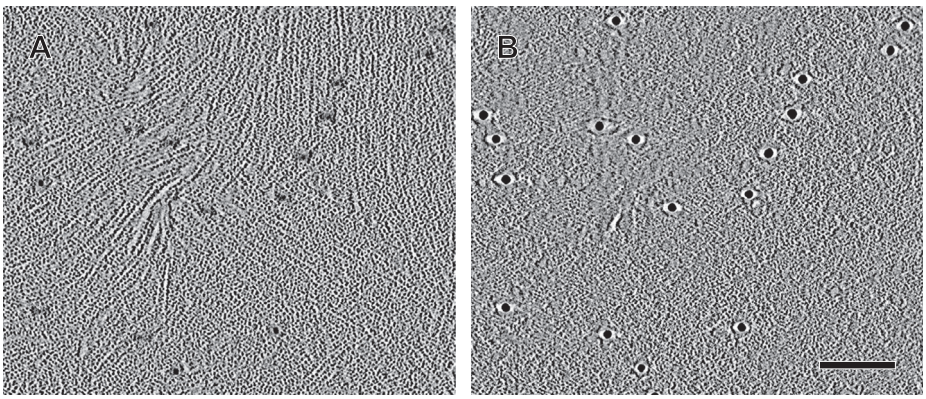

Fig.2. Selected slices from a tomographic reconstruction of a chaplin film assembled at the air–water interface after rotation-shadowing with Pt. The slices are separated by 2.4 nm. The slice in (A) is near the hydrophobic surface. The slice in (B) indicates the hydrophilic surface where the fiducial markers are located. The scale bar represents 100 nm.

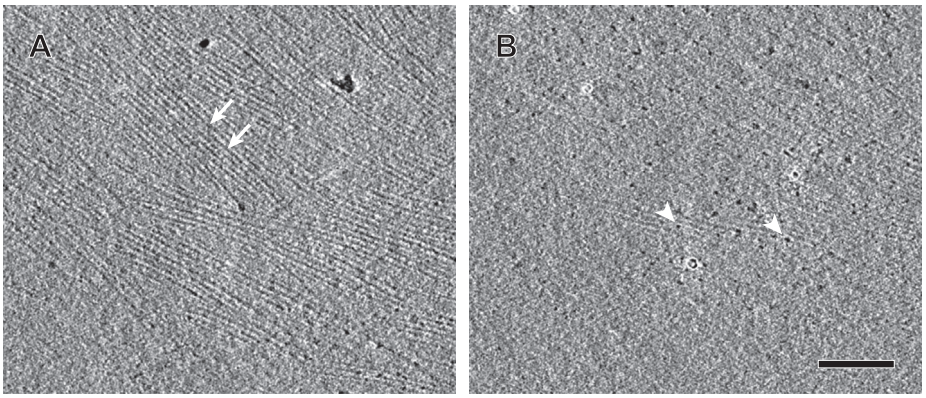

Fig.3. Selected slices from a tomographic reconstruction of chaplin film assembled at the air–water interface embedded in vitreous ice. The slices are separated by 7.0 nm. The slice in (A) is near the hydrophobic surface. Arrows indicate the fibrillar organization of the film at this level. Arrow heads in (B) indicate the presence of small protrusions at the hydrophilic surface. The scale bar represents 100 nm.

electron diffraction patterns we never observed a meridional reflection at 0.94 nm, which indicated that the β-strands are most likely arranged in a parallel, rather than in an anti-parallel fashion.

3.3. Chaplins assemble into distinct amyloid-like fibrillar structures in solution

It was previously shown that monomeric chaplins assemble in aqueous solutions (de Jong et al., 2009). However, no detailed ultrastructural information is available for chaplins assembled in this manner. When a dilute chaplin solution (~5–20 μg protein/ml) was incubated for 7 days, long (several micrometers) fibrils with a constant diameter of 12 nm were formed (Fig. 7A), as opposed to the 7.3 nm fibrils formed at the air–water interface. Occasionally these 12 nm-wide fibrils appear unwound (arrows in Fig. 7A and S3) and show thinner fibrils with a diameter of approximately 7 nm (arrowheads in Fig. 7A and S3). Single particle image analysis was applied to find further details in these fibrillar structures by averaging small frames of fibrils. Occasionally a weak hint of a helical organization was observed in the calculated diffraction pattern from selected fibril segments. However, the observed helical parameters (layer line distance and intensities) were too variable between segments to deduce any generalized helical organization.

To see if the chaplin fibrils formed in solution are also amyloid, electron diffraction patterns of frozen hydrated samples were recorded, followed by electron imaging of the same area. The diffractogram in Fig. 7B shows the presence of a strong reflection at 1/0.47 nm^{-1} in the direction of the fibril axis, similar to that of

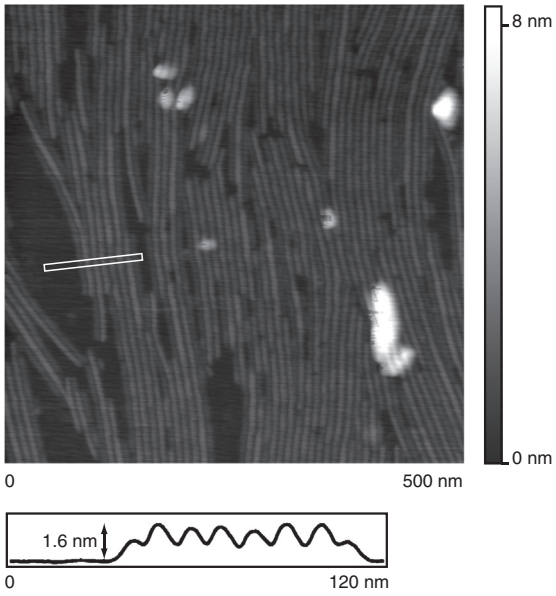

Fig.4. Atomic force microscopy of the air-exposed side of the chaplin film mounted on mica reveals fibrils with a diameter of 7–8 nm. These fibrils are ±1.6 nm high based on the height profile of a cross section averaged along the length of fibrils in the boxed area.

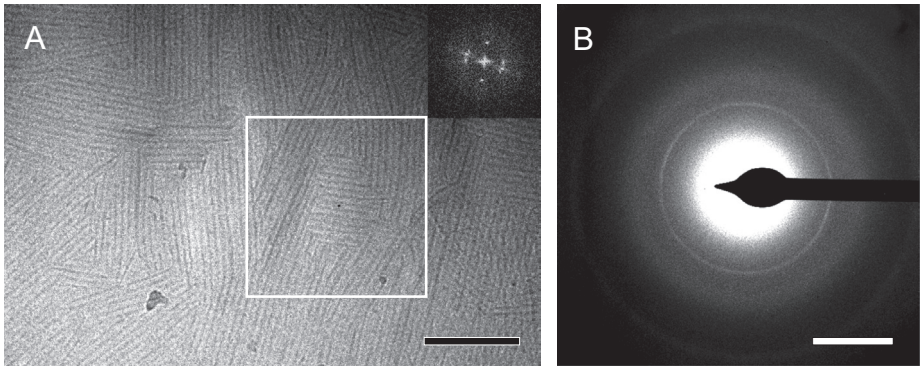

Fig.5. Cryo-electron microscopy and diffraction of chaplin films. (A) Cryo-electron micrograph of a frozen hydrated chaplin film spanning a hole in a carbon support film. Inset: diffraction pattern calculated from the boxed area. Reflections are visible at 1/7.3 nm^{-1} in different orientations, corresponding to the side-by-side packing distance of the fibrils. Scale bar represents 100 nm. (B) Selected area electron diffraction pattern from a frozen hydrated film as in A. The sharp diffraction ring at 1/4.7 nm^{-1} comes from the β-strand packing in the fibrils in random orientation. The scale bar represents 2 nm^{-1}.

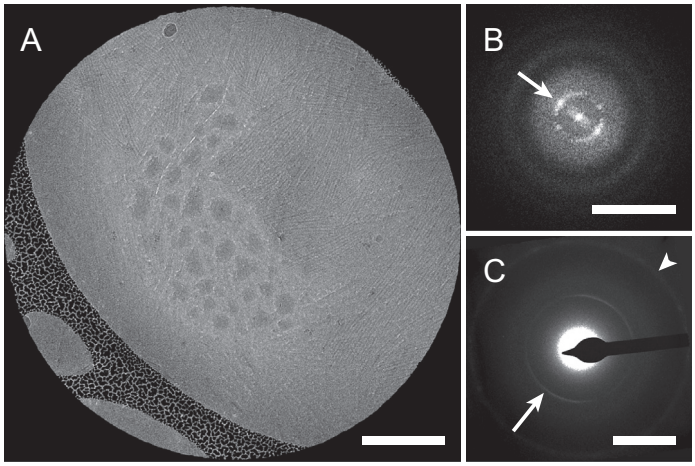

Fig.6. Combined electron diffraction and imaging of a frozen-hydrated, unstained chaplin fiber layer. (A) cryo-TEM micrograph of a layer over a hole in the support film. Scale bar represents 200 nm. (B) Calculated diffraction pattern of the upper right chaplin fiber-rich area of the image of frame A. The arrow points at reflections at 1/7.3 nm^{-1}, which comes from the side-by-side packing of the fibers. Scale bar represents 0.5 nm^{-1}. (C) Selected area electron diffraction pattern of the area of frame A. The sharp ring at 1/0.47 nm^{-1}, corresponds to distances of 0.47 nm between β-strands in a β-sheet (arrow). The ring at 1/0.235 nm^{-1} is from gold, an internal standard that has been evaporated onto the backside of the carbon prior to addition of the protein solution (arrowhead). Scale bar 2.5 nm^{-1}.

fibrils assembled at the air–water interface. These data show that chaplins assemble in solution into distinct hydrophilic amyloid structures.

4. Discussion

We characterized chaplin fibril films formed at the air–water interface, which was proposed to occur *in vivo*, and which also mimics the situation when chaplins assemble on the interface between the (hydrophilic) cell wall and the air (Claessen et al., 2004). Shadowing experiments from both sides of the chaplin film gave conclusive evidence that the fibril structures formed by the chaplin proteins are highly asymmetric. The hydrophobic side of the film, facing the air, is curved while the hydrophilic side is rather flat and unstructured (Fig. 1). Using Cryo-EM, the fibril diameter was shown to be 7.3 nm and our cryo electron tomographic reconstruction showed that the native hydrated chaplin film is 7 nm thick. Based on our experimental data we postulate a model for the structural arrangement of chaplins in the fibril film. Electron diffraction experiments showed the presence of a spacing of 0.47 nm, while correlative diffraction/imaging experiments proved that this spacing is in the direction of the fiber axis, consistent with an amyloid cross-β structure. The β-strands lie perpendicular to the fibril axis, while hydrogen bond interaction between neighboring strands results in the formation of a continuous β-sheet in the direction of the fibril. Secondary structure predictions using PsiPred (Jones, 1999) showed that 17 core residues in the chaplins have the tendency to form β-strands that contribute to β-sheet formation in the fibril, while the termini are likely to form random coil segments (Fig. S4A). A hydrophilicity profile (Hopp and Woods, 1981) shows that these random coil segments are hydrophilic, while the β-stranded core is hydrophobic. This amphipatic nature explains how chaplins self-assemble at the air–water interface, during which the hydrophilic termini orient towards the solvent while the β-stranded core is exposed to the air (Fig. 8A). Furthermore, every chaplin molecule, except for ChpE, has two cysteines that are possibly engaged in a disulfide bridge (Elliot et al., 2003; Di Berardo et al., 2008). In our model this disulfide bridge connects the C-terminal segment and the central β-strand to maintain a compact and rigid structure (Fig. 8B).Whether ChpE, which lacks Cys residues, has a special role in this respect remains to be established.

The curved hydrophobic side of the chaplin fiber would have a circumference of approximately 17 nm that cannot be spanned by the 17 core residues forming β-strands from a single chaplin molecule [approximately 5 nm in length given 0.33 nm per β-stranded residue (Mao et al., 2009)]. Therefore, we propose that two chaplin molecules, oriented in a head-to-head fashion, form the repeating

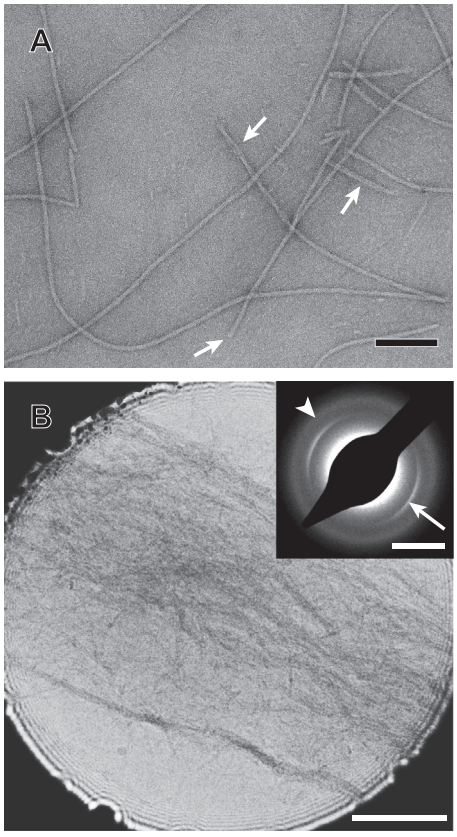

Fig.7. Electron microscopy and diffraction of chaplin assemblies formed in solution. (A) Long fibers formed at low protein concentration after 1 week of incubation as visualized by negative staining with uranyl acetate. The scale bar is 100 nm. Arrows indicate unwound and flattened fibrous aggregates; the arrowhead indicates a single or double fibril emanating from a larger aggregate. (B) Electron image of frozen hydrated chaplin fibers formed in solution, with a diffraction pattern (inset) of the same area. The arrow points at the 1/0.47 nm^{-1} reflection arising from the cross-β structure, the arrowhead indicates the diffuse ring coming from amorphous ice. Bar 200 nm (image) and 2 nm^{-1} (diffractogram).

unit of the fiber (Fig. 8A and B). Stacking of these repeating units in the direction of the fibril axis results in a large β-sheet via hydrogen bonding interactions (indicated in red in Fig. 8B). Fibrils probably only contain parallel β-sheets, which is based on the electron diffraction data that show a strong peak at 1/0.47 nm^{-1} while a 1/0.96 nm^{-1} peak (for anti-parallel β-sheets, (Serpell and Smith, 2000; Makin and Serpell, 2005) is absent (Figs. 5B and 6C).

Our model is very different from the high symmetry that is observed in many helical, cylindrical or twisted ribbon-like hydrophilic amyloids that are associated with diseases like Alzheimer, type II diabetes, Parkinson and Creutzfeld-Jacob (Chiti and Dobson, 2006) and in functional amyloids like curli (Wang et al., 2008). Therefore, in this functional form chaplins more resemble the fungal hydrophobins (de Vocht et al., 2002; Szilvay et al., 2007) which are also amphipathic and capable of assembling at hydrophobic–hydrophilic interfaces (Wösten et al., 1994a,b; Wösten et al., 1993). However, they are structurally non-related: the primary structure and predicted secondary structure elements show no resemblance, and the number and distribution of conserved disulfide bridges is different (Hakanpaa et al., 2004; Kwan et al., 2006).

It should be noted that this *in vitro* system lacks ChpA, ChpB and ChpC. These long chaplins are thought to be covalently coupled to the peptidoglycan layer and therefore cannot be extracted with TFA. Because ChpA–C contain two chaplin domains (Claessen et al., 2003), we propose that *in vivo* the repeating unit in the fibrils occasionally comprises one large chaplin instead of two small ones. Thereby the large chaplins are able to anchor the fibril film to the bacterial surface whilst also contributing to the formation of the fibrillar layer itself. The long chaplins are not required for the assembly of rodlets though, as the *chpABCDEH* strain *in vivo* formed rodlets indistinguishable from those in the wild-type strain (Claessen et al., 2004). Furthermore, it has been shown that synthetically synthesized small chaplins are capable of forming amyloid structures individually (Sawyer et al., 2011) without the need for any of the other chaplins. Why *S. coelicolor* shows this apparent redundancy for the chaplin proteins requires further investigation.

4.1. Two distinct functional amyloid structures

The 12 nm chaplin fibrils formed in solution strongly resemble the fimbrial structures found on the cell surface of adhering hyphae of *S. coelicolor* (de Jong et al., 2009) and amyloid fibers formed by various other proteins (Jiménez et al., 1999). Moreover, the cross-β structure observed by electron diffraction provides direct evidence that the hydrophilic chaplin fibrils formed in solution are also amyloid in nature. It is remarkable that chaplins assemble

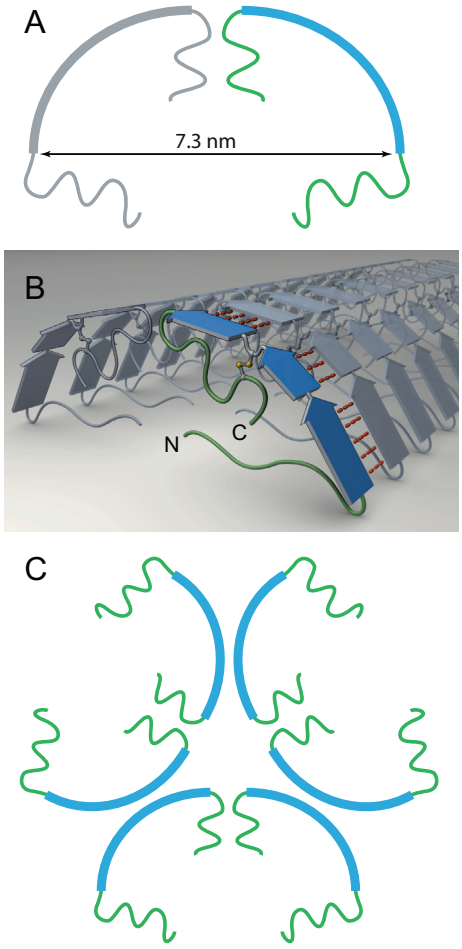

Fig.8. Proposed model for the amphiphilicchaplin amyloid fiber. (A) A chaplin fiber is 7.3 nm wide and contains two small chaplins per repeating unit. The hydrophilic loops (green) are submerged in the solvent, while the β-strands (blue) are air-exposed. (B) The two chaplins in the repeating unit are related by a twofold axis. Red dashes indicate hydrogen bonds in the fiber plane that form between the β-strands of the chaplin upon parallel β-sheet formation that give rise to a 1/0.47 nm^{-1} reflection in an electron diffraction pattern. (C) A model in which three 7.3 nm wide fibrils assemble into the 12 nm fibers formed in solution. The hydrophobic surface of the β-strand is buried within the fiber, while the hydrophilic loops are exposed to the solvent.

into two different amyloid forms, both being functional in nature. There is a vast amount of data on the influence of environmental factors, such as amongst others hydrophobicity, temperature and pH on amyloid fibril structure (Zhu et al., 2002; Keller et al., 2011). However, in this work we present different structural states of the prokaryotic chaplin amyloids induced by its microenvironment that reflect two different biologically relevant situations. One, the amphipathic fibril film resembling the amphipathic amyloidal membrane formed by fungal hydrophobins, and the other fibrillar hydrophilic structures that mediate attachment of *S. coelicolor* to surfaces (de Jong et al., 2009), mostly resembling bacterial adhesion structures. In these fimbriae the hydrophobic surface of the β-strands must be buried inside the fibrils. This can be envisaged by association of different (3–5) fibrils with the hydrophilic surface facing outward, as illustrated schematically in Fig. 8C. However, we cannot exclude that the 12 nm fibers originate from a drastic conformational change of the monomer. Adhesion of fimbriae to hydrophobic substrates would require partial unfolding or unwinding of the fibrils to expose a hydrophobic surface of the protein. Indeed, electron micrographs show that the fibril bundles occasionally appear unwound forming flattened structures or exposing single fibers (Fig. 7A and S3). The threefold symmetrical fibril arrangement of the chaplins in the fibrillar aggregates is similar to the arrangement proposed for the prions (Govaerts et al., 2004). Although in both the chaplin- and prion-model the β-strands assemble back-to-back, the 1–1.2 nm repeat associated with β-sheet stacking is absent (Wille et al., 2009). This suggests that the fibril organization is different from most filamentous amyloids (Jahn et al., 2010).

Acknowledgments

We are grateful to Martin G. Faber (Zernike Institute for Advanced Materials, Faculty of Mathematics and Natural Sciences, University of Groningen, The Netherlands) for his help with the atomic force microscopy.

Appendix A. Supplementary data

Supplementary data associated with this article can be found, in the online version, at http://dx.doi.org/10.1016/j.jsb.2013.08.013.

References

Alteri, C.J., Xicohtencatl-Cortes, J., Hess, S., Caballero-Olin, G., Giron, J.A., et al., 2007. *Mycobacterium tuberculosis* produces pili during human infection. Proc. Natl. Acad. Sci. USA 104, 5145–5150.

Chiti, F., Dobson, C.M., 2006. Protein misfolding, functional amyloid, and human disease. Annu. Rev. Biochem. 75, 333–366.

Claessen, D., Rink, R., de Jong, W., Siebring, J., de Vreugd, P., et al., 2003. A novel class of secreted hydrophobic proteins is involved in aerial hyphae formation in *Streptomyces coelicolor* by forming amyloid-like fibrils. Genes Dev. 17, 1714–1726.

Claessen, D., Stokroos, I., Deelstra, H.J., Penninga, N.A., Bormann, C., et al., 2004. The formation of the rodlet layer of streptomycetes is the result of the interplay between rodlins and chaplins. Mol. Microbiol. 53, 433–443.

Claessen, D., Wösten, H.A.B., van Keulen, G., Faber, O.G., Alves, A.M.C.R., et al., 2002. Two novel homologous proteins of *Streptomyces coelicolor* and *Streptomyces lividans* are involved in the formation of the rodlet layer and mediate attachment to a hydrophobic surface. Mol. Microbiol. 44, 1483–1492.

de Jong, W., Wösten, H.A.B., Dijkhuizen, L., Claessen, D., 2009. Attachment of *Streptomyces coelicolor* is mediated by amyloidal fimbriae that are anchored to the cell surface via cellulose. Mol. Microbiol. 73, 1128–1140.

de Vocht, M.L., Reviakine, I., Ulrich, W.P., Bergsma-Schutter, W.G., Wösten, H.A.B., et al., 2002. Self-assembly of the hydrophobin SC3 proceeds via two structural intermediates. Protein Sci. 11, 1199–1205.

Del Sol, R., Armstrong, I., Wright, C., Dyson, P., 2007. Characterization of changes to the cell surface during the life cycle of *Streptomyces coelicolor*: atomic force microscopy of living cells. J. Bact. 189, 2219–2225.

Di Berardo, C., Capstick, D.S., Bibb, M.J., Findlay, K.C., Buttner, M.J., et al., 2008. Function and redundancy of the chaplin cell surface proteins in aerial hypha formation, rodlet assembly, and viability in *Streptomyces coelicolor*. J. Bact. 190, 5879–5889.

Duong, A., Capstick, D.S., Di Berardo, C., Findlay, K.C., Hesketh, A., et al., 2012. Aerial development in *Streptomyces coelicolor* requires sortase activity. Mol. Microbiol. 83, 992–1005.

Eanes, E.D., Glenner, G.G., 1968. X-ray diffraction studies on amyloid filaments. J. Histochem. Cytochem. 16, 673–677.

Eisenberg, D., Nelson, R., Sawaya, M.R., Balbirnie, M., Sambashivan, S., et al., 2006. The structural biology of protein aggregation diseases: fundamental questions and some answers. Acc. Chem. Res. 39, 568–575.

Elliot, M.A., Karoonuthaisiri, N., Huang, J.Q., Bibb, M.J., Cohen, S.N., et al., 2003. The chaplins: a family of hydrophobic cell-surface proteins involved in aerial mycelium formation in *Streptomyces coelicolor*. Genes Dev. 17, 1727–1740.

Epstein, E.A., Chapman, M.R., 2008. Polymerizing the fibre between bacteria and host cells: the biogenesis of functional amyloid fibres. Cell. Microbiol. 10, 1413–1420.

Flärdh, K., Buttner, M.J., 2009. *Streptomyces* morphogenetics: dissecting differentiation in a filamentous bacterium. Nat. Rev. Microbiol. 7, 36–49.

Fowler, D.M., Koulov, A.V., Balch, W.E., Kelly, J.W., 2007. Functional amyloid – from bacteria to humans. Trends Biochem. Sci. 32, 217–224.

Govaerts, C., Wille, H., Prusiner, S.B., Cohen, F.E., 2004. Evidence for assembly of prions with left-handed beta 3-helices into trimers. Proc. Natl. Acad. Sci. USA 101, 8342–8347.

Hakanpaa, J., Paananen, A., Askolin, S., Nakari-Setala, T., Parkkinen, T., et al., 2004. Atomic resolution structure of the HFBII hydrophobin, a self-assembling amphiphile. J. Biol. Chem. 279, 534–539.

Hopp, T.P., Woods, K.R., 1981. Prediction of protein antigenic determinants from amino-acid-sequences. Proc. Natl. Acad. Sci. USA 78, 3824–3828.

Jahn, T.R., Makin, O.S., Morris, K.L., Marshall, K.E., Tian, P., et al., 2010. The common architecture of cross-beta amyloid. J. Mol. Biol. 395, 717–727.

Jiménez, J.L., Guijarro, J.L., Orlova, E., Zurdo, J., Dobson, C.M., et al., 1999. Cryo-electron microscopy structure of an SH3 amyloid fibril and model of the molecular packing. EMBO J. 18, 815–821.

Jones, D.T., 1999. Protein secondary structure prediction based on position-specific scoring matrices. J. Mol. Biol. 292, 195–202.

Keller, A., Fritzsche, M., Yu, Y., Liu, Q., Li, Y., et al., 2011. Influence of hydrophobicity on the surface-catalyzed assembly of the islet amyloid polypeptide. ACS Nano 5, 2770–2778.

Kirschner, D.A., Inouye, H., Duffy, L.K., Sinclair, A., Lind, M., et al., 1987. Synthetic peptide homologous to beta-protein from alzheimer-disease forms amyloid-like fibrils *in vitro*. Proc. Natl. Acad. Sci. USA 84, 6953–6957.

Kodani, S., Hudson, M.E., Durrant, M.C., Buttner, M.J., Nodwell, J.R., et al., 2004. The SapBmorphogen is a lantibiotic-like peptide derived from the product of the developmental gene ramS in *Streptomyces coelicolor*. Proc. Natl. Acad. Sci. USA 101, 11448–11453.

Kremer, J.R., Mastronarde, D.N., McIntosh, J.R., 1996. Computer visualization of three-dimensional image data using IMOD. J. Struct. Biol. 116, 71–76.

Kwan, A.H., Macindoe, I., Vukasin, P.V., Morris, V.K., Kass, I., et al., 2008. The Cys3-Cys4 loop of the hydrophobin EAS is not required for rodlet formation and surface activity. J. Mol. Biol. 382, 708–720.

Kwan, A.H.Y., Winefield, R.D., Sunde, M., Matthews, J.M., Haverkamp, R.G., et al., 2006. Structural basis for rodlet assembly in fungal hydrophobins. Proc. Natl. Acad. Sci. USA 103, 3621–3626.

Makin, O.S., Serpell, L.C., 2005. Structures for amyloid fibrils. FEBS J. 272, 5950–5961.

Mao, X., Ma, X., Liu, L., Niu, L., Yang, Y., et al., 2009. Structural characteristics of the beta-sheet-like human and rat islet amyloid polypeptides as determined by scanning tunneling microscopy. J. Struct. Biol. 167, 209–215.

Maury, C.P.J., 2009. The emerging concept of functional amyloid. J. Intern. Med. 265, 329–334.

Necas, D., Klapetek, P., 2012. Gwyddion: an open-source software for SPM data analysis. Cent. Eur. J. Phys. 10, 181–188.

Otzen, D., Nielsen, P.H., 2008. We find them here, we find them there: functional bacterial amyloid. Cell Mol. Life Sci. 65, 910–927.

Podrabsky, J.E., Carpenter, J.F., Hand, S.C., 2001. Survival of water stress in annual fish embryos: dehydration avoidance and egg envelope amyloid fibers. Am. J. Physiol. Regul. Integr. Comp. Physiol. 280, 123–R131.

Ritter, C., Maddelein, M.L., Siemer, A.B., Luhrs, T., Ernst, M., et al., 2005. Correlation of structural elements and infectivity of the HET-s prion. Nature 435, 844–848.

Sawyer, E.B., Claessen, D., Haas, M., Hurgobin, B., Gras, S.L., 2011. The assembly of individual chaplin peptides from *Streptomyces coelicolor* into functional amyloid fibrils. PLoS One 6, e18839.

Serpell, L.C., 2000. Alzheimer's amyloid fibrils: structure and assembly. Biochim. Biophys. Acta, Mol. Basis Dis. 1502, 16–30.

Serpell, L.C., Smith, J.M., 2000. Direct visualisation of the beta-sheet structure of synthetic Alzheimer's amyloid. J. Mol. Biol. 299, 225–231.

Shewmaker, F., McGlinchey, R.P., Thurber, K.R., McPhie, P., Dyda, F., et al., 2009. The functional curli amyloid is not based on in-register parallel β-sheet structure. J. Biol. Chem. 284, 25065–25076.

Stefani, M., 2004. Protein misfolding and aggregation: new examples in medicine and biology of the dark side of the protein world. Biochim. Biophys. Acta, Mol. Basis Dis. 1739, 5–25.

Sunde, M., Serpell, L.C., Bartlam, M., Fraser, P.E., Pepys, M.B., et al., 1997. Common core structure of amyloid fibrils by synchrotron X-ray diffraction. J. Mol. Biol. 273, 729–739.
Szilvay, G.R., Paananen, A., Laurikainen, K., Vuorimaa, E., Lemmetyinen, H., et al., 2007. Self-assembled hydrophobin protein films at the air–water interface: structural analysis and molecular engineering. Biochemistry 46, 2345–2354.
Wang, X., Hammer, N.D., Chapman, M.R., 2008. The molecular basis of functional bacterial amyloid polymerization and nucleation. J. Biol. Chem. 283, 21530–21539.
Wasmer, C., Lange, A., Van Melckebeke, H., Siemer, A.B., Riek, R., et al., 2008. Amyloid fibrils of the HET-s(218–289) prion form a beta solenoid with a triangular hydrophobic core. Science 319, 1523–1526.
Wille, H., Bian, W., McDonald, M., Kendall, A., Colby, D.W., et al., 2009. Natural and synthetic prion structure from X-ray fiber diffraction. Proc. Natl. Acad. Sci. USA 106, 16990–16995.
Willey, J., Santamaria, R., Guijarro, J., Geistlich, M., Losick, R., 1991. Extracellular complementation of a developmental mutation implicates a small sporulation protein in aerial mycelium formation by *S. coelicolor*. Cell 65, 641–650.
Willey, J., Schwedock, J., Losick, R., 1993. Multiple extracellular signals govern the production of a morphogenetic protein involved in aerial mycelium formation by *Streptomyces coelicolor*. Genes Dev. 7, 895–903.
Wösten, H.A.B., Asgeirsdottir, S.A., Krook, J.H., Drenth, J.H.H., Wessels, J.G.H., 1994a. The fungal hydrophobin Sc3p self-assembles at the surface of aerial hyphae as a protein membrane constituting the hydrophobic rodlet layer. Eur. J. Cell Biol. 63, 122–129.
Wösten, H.A.B., De Vries, O.M.H., Wessels, J.G.H., 1993. Interfacial self-assembly of a fungal hydrophobin into a hydrophobic rodlet layer. Plant Cell 5, 1567–1574.
Wösten, H.A.B., Schuren, F.H.J., Wessels, J.G.H., 1994b. Interfacial self-assembly of a hydrophobin into an amphipathic protein membrane mediates fungal attachment to hydrophobic surfaces. EMBO J. 13, 5848–5854.
Zhu, M., Souillac, P., Ionescu-Zanetti, C., Carter, S., Fink, A., 2002. Surface-catalyzed amyloid fibril formation. J. Biol. Chem. 277, 50914–50922.